



Quantum Computation and Quantum Chaos

Dima Shepelyansky

CNRS Toulouse, FR (www.quantware.ups-tlse.fr)



Objective

- Effects of realistic imperfections on quantum computer operability and accuracy
- Decoherence and quantum chaos induced by inter-qubit couplings
- New efficient algorithms for simulation of quantum and classical physical systems
- Numerical codes with up to 30 qubits
- Development and test of error-correcting codes for quantum chaos and noisy gates



Objective Approach

- Analytical methods developed for many-body systems (nuclei, atoms, quantum dots)
- Random matrix theory and quantum chaos
- Large-scale numerical simulations of many qubits on modern supercomputers
- Stability of algorithms to quantum errors

Status

- The Great Wave of Quantum Chaos (by Katsushika Hokusai)
- RMT for quantum computations, universal law for fidelity decay induced by imperfections
- New quantum algorithms and imperfection effects for chaos maps, Grover algorithm; numerics with 7-28 qubits; Cory experiment

Quantware group at Toulouse

Laboratoire de Physique Théorique
UMR 5152 du CNRS, Université Paul Sabatier
Toulouse, France www.quantware.ups-tlse.fr

R.Fleckinger, K.Frahm, D.Braun (professors Univ. P.Sabatier)

D.L.Shepelyansky (PI), B. Georgeot, O.Giraud (researchers CNRS)

I. García-Mata (post-doc EC IST-FET EuroSQIP)

A.D.Chepelianskii (undergraduate ENS)

Collaboration: O.V.Zhirov (Budker Inst. of Nuclear Physics, Novosibirsk)

SUPPORT: EC IST-FET project EuroSQIP

Elementary quantum gates

PHYSICAL REVIEW A

VOLUME 54, NUMBER 1

JULY 1996

Quantum networks for elementary arithmetic operations

Vlatko Vedral,^{*} Adriano Barenco, and Artur Ekert

Clarendon Laboratory, Department of Physics, University of Oxford, Oxford OX1 3PU, United Kingdom

(Received 3 November 1995)

Quantum computers require quantum arithmetic. We provide an explicit construction of quantum networks effecting basic arithmetic operations: from addition to modular exponentiation. Quantum modular exponentiation seems to be the most difficult (time and space consuming) part of Shor's quantum factorizing algorithm. We show that the auxiliary memory required to perform this operation in a reversible way grows linearly with the size of the number to be factorized. [S 1050-2947(96)05707-1]

PACS number(s): 03.65.Ca, 07.05.Bx, 89.80.+h

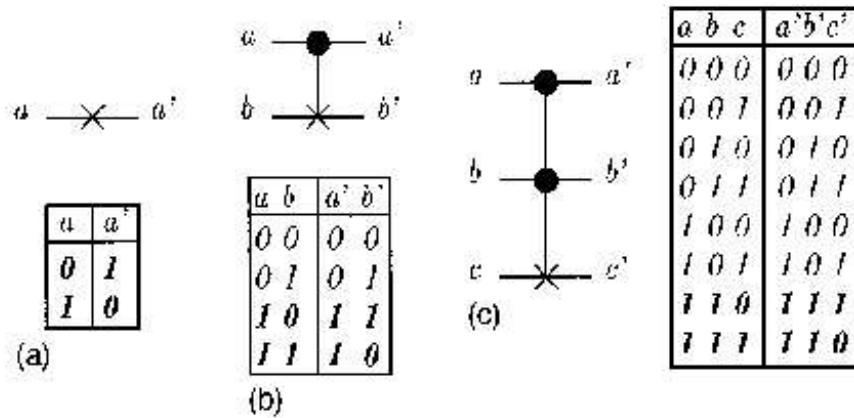


FIG. 1. Truth tables and graphical representations of the elementary quantum gates used for the construction of more complicated quantum networks. The control qubits are graphically represented by a dot, the target qubits by a cross. (a) NOT operation. (b) control-NOT. This gate can be seen as a “copy operation” in the sense that a target qubit (b) initially in the state 0 will be after the action of the gate in the same state as the control qubit. (c) Toffoli gate. This gate can also be seen as a control-control-NOT: the target bit (c) undergoes a NOT operation only when the two controls (a and b) are in state 1.

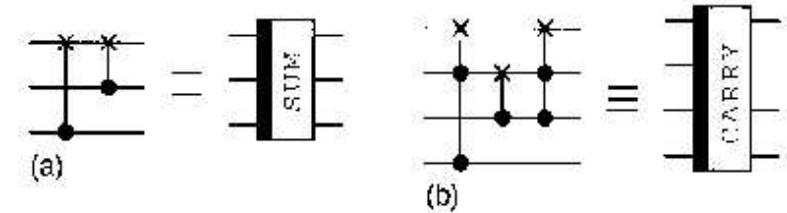
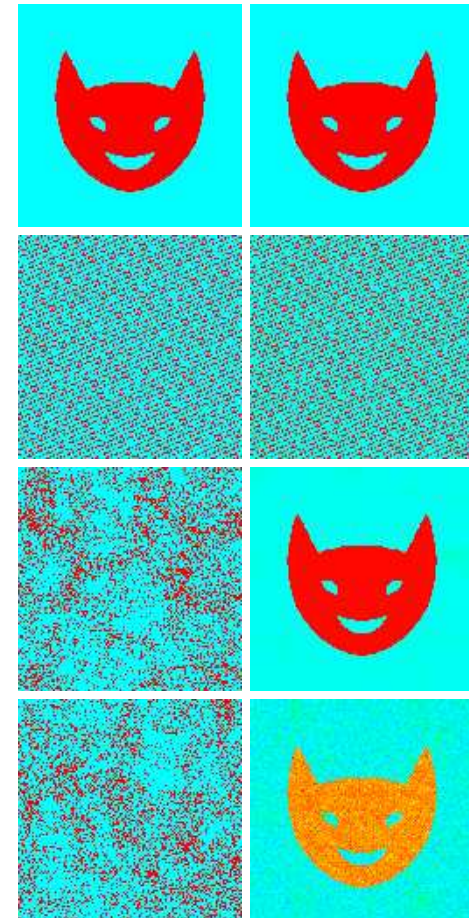


FIG. 3. Basic carry and sum operations for the plain addition network. (a) the carry operation (note that the carry operation perturbs the state of the qubit b). (b) the sum operation.

Talk Overview

- * Quantum computer hardware: static properties, imperfections effects
- * Quantum algorithms of simple classical/quantum maps: tent map, Arnold cat map, sawtooth map, Chirikov standard map (polynomial number of gates)
- * Effects of imperfections and errors, fidelity decay: tent map, sawtooth map, Grover, Shor algorithms
- * Experiment of Cory group at MIT: dynamical localization in the quantum sawtooth map



Arnold cat map on QC with 20 qubits (128×128), time inversion after 10 and 200 iterations.

Quantum Hardware Melting Induced by Quantum Chaos

The quantum computer hardware is modeled as a (one)two-dimensional lattice of qubits (spin halves) with static fluctuations/imperfections in the individual qubit energies and residual short-range inter-qubit couplings. The model is described by the many-body Hamiltonian (B.Georgeot, DS, PRE **62**, 3504 (2000)):

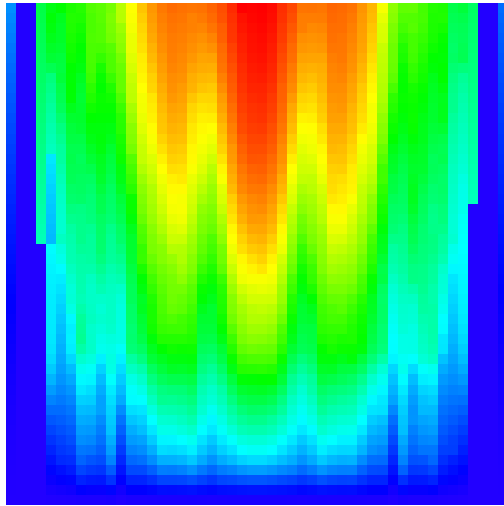
$$H_S = \sum_i (\Delta_0 + \delta_i) \sigma_i^z + \sum_{i < j} J_{ij} \sigma_i^x \sigma_j^x,$$

where the σ_i are the Pauli matrices for the qubit i , and Δ_0 is the average level spacing for one qubit. The second sum runs over nearest-neighbor qubit pairs, and δ_i , J_{ij} are randomly and uniformly distributed in the intervals $[-\delta/2, \delta/2]$ and $[-J, J]$, respectively. **Quantum chaos border for quantum hardware:**

$$J > J_c \approx \Delta_c \approx 3\delta/n_q \gg \Delta_n \sim \delta 2^{-n_q}$$

Emergency rate of quantum chaos: $\Gamma \sim J^2/\Delta_c$.

(Yamamoto QC with mag field gradient: J.Lages, DS, PRE **74**, 026208 (2006))



Quantum computer melting induced by inter-qubit couplings. Color represents the level of quantum eigenstate entropy S_q (red for maximum $S_q \approx 11$, blue for minimum $S_q = 0$). Horizontal axis is the energy of the computer eigenstates counted from the ground state to the maximal energy ($\approx 2n_q\Delta_0$). Vertical axis gives the value of J/Δ_0 (from 0 to 0.5). Here $n_q = 12$, $J_c/\Delta_0 = 0.273$, and one random realization of couplings is chosen.

What are effects of quantum many-body chaos on the accuracy of quantum computations?
Static imperfections vs. random errors in quantum gates of a quantum algorithm.

Fidelity decay due to errors

Accuracy measure of quantum computation is fidelity: $f(t) = |\langle \psi(t) | \psi_\varepsilon(t) \rangle|^2$.

Quantum algorithm: $|\psi(t)\rangle = U^t |\psi(0)\rangle$, $U = \underbrace{U_{N_g} \cdot \dots \cdot U_1}_{\text{elementary gates}}$.

Errors: $U_j \rightarrow U_j e^{i\delta H}$, $\delta H \sim \varepsilon$.

(i) Decoherence due to residual couplings of quantum computer to external bath:

δH random and different at each j and t ,

e.g.: random phase fluctuations: $\delta\phi \in [-\varepsilon, \varepsilon]$ in phase-shift gates.

(ii) Static imperfections in the quantum computer itself:

δH (random but) constant at each j and t ,

e.g.:
$$\delta H = \sum_{j=0}^{n_q-1} \delta_j \sigma_j^{(z)} + 2 \sum_{j=0}^{n_q-2} J_j \sigma_j^{(x)} \sigma_{j+1}^{(x)}, \quad J_j, \delta_j \in [-\varepsilon, \varepsilon].$$

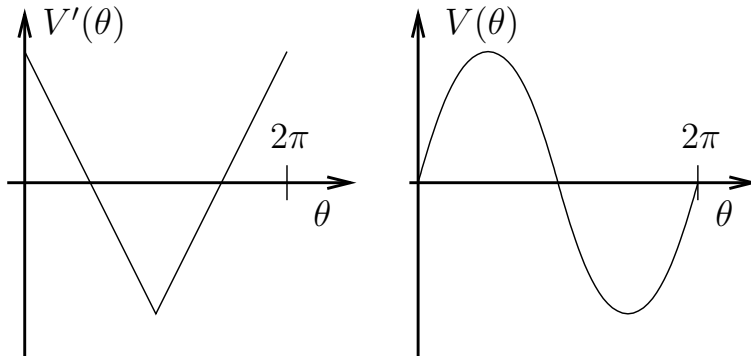
(iii) Non-unitary errors in quantum computation:

$e^{i\delta H}$ is non-unitary ($\delta H \neq \delta H^\dagger$, density matrix and quantum trajectories approach,

J.W.Lee, DS, PRE **71**, 056202 (2005))

Example: model of quantum tent map

$$H(t) = \frac{T p^2}{2} + V(\theta) \sum_{n=-\infty}^{\infty} \delta(t - n)$$



Classical map :

$$p_{n+1} = p_n - V'(\theta_n)$$

$$\theta_{n+1} = \theta_n + T p_{n+1}$$

Quantum map : $p = -i\partial/\partial\theta$

$$|\psi(t+1)\rangle = U |\psi(t)\rangle$$

$$U = e^{-iT p^2/2} e^{-iV(\theta)}$$

$$V(\theta) = \begin{cases} -\frac{k}{2}\theta(\theta - \pi) & \text{if } 0 \leq \theta \leq \pi \\ \frac{k}{2}(\theta - \pi)(\theta - 2\pi) & \text{if } \pi \leq \theta \leq 2\pi \end{cases}, \quad V'(\theta) = \begin{cases} k(\frac{\pi}{2} - \theta) & \text{if } 0 \leq \theta \leq \pi \\ k(-\frac{3\pi}{2} + \theta) & \text{if } \pi \leq \theta \leq 2\pi \end{cases}$$

Quantum algorithm for tent (and sawtooth) map

Quantum register identification: $|p\rangle \equiv |\alpha_0\rangle_0 |\alpha_1\rangle_1 \dots |\alpha_{n_q-1}\rangle_{n_q-1}$.

$$p = \sum_{j=0}^{n_q-1} \alpha_j 2^j \in \{0, \dots, N - 1\}$$

$N = 2^{n_q}$ = dimension of Hilbert space; n_q = number of qubits; $\alpha_j \in \{0, 1\}$.

Quantum Fourier transform: $p \leftrightarrow \theta$ and $e^{-iT p^2/2} |p\rangle = \prod_{j < k} \underbrace{e^{i(\dots)\alpha_j \alpha_k}}_{B_{jk}^{(2)}(\dots)} \prod_j \underbrace{e^{i(\dots)\alpha_j}}_{B_j^{(1)}(\dots)} |p\rangle$.

with simple and controlled phase-shift:

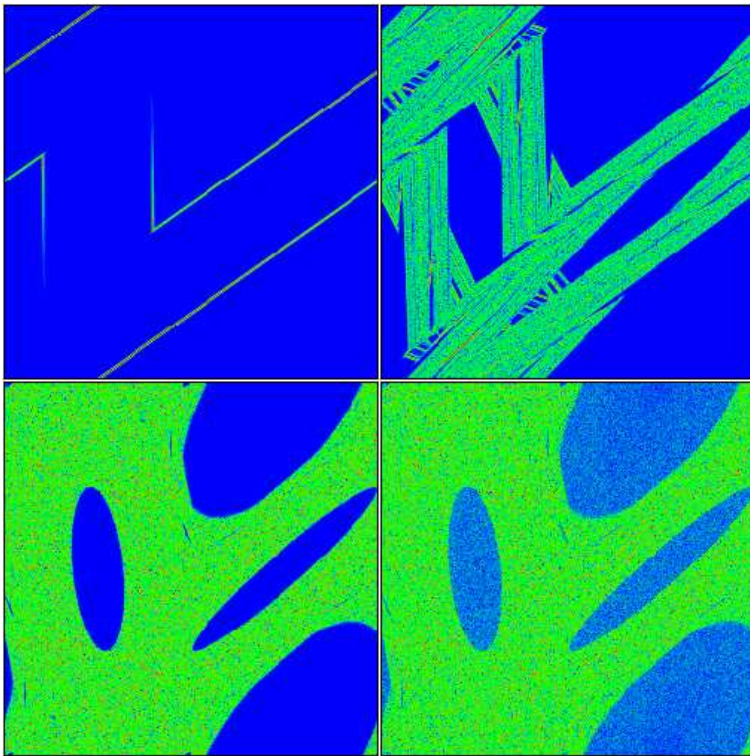
$$B_j^{(1)}(\phi) = \begin{pmatrix} 1 & 0 \\ 0 & e^{i\phi} \end{pmatrix}, \quad B_{jk}^{(2)}(\phi) = \begin{pmatrix} 1 & 0 & 0 & 0 \\ 0 & 1 & 0 & 0 \\ 0 & 0 & 1 & 0 \\ 0 & 0 & 0 & e^{i\phi} \end{pmatrix} .$$

Double controlled phase-shift: $B_{jkl}^{(3)}(\phi) = B_{jl}^{(2)}\left(\frac{\phi}{2}\right) B_{jk}^{(2)}\left(\frac{\phi}{2}\right) C_{kl}^{(N)} B_{jk}^{(2)}\left(-\frac{\phi}{2}\right) C_{kl}^{(N)}$.

Number of elementary gates: $n_g \approx 9 n_q^2/2$

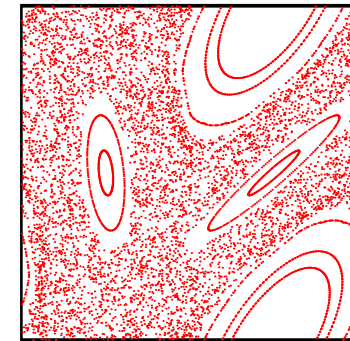
Husimi function

$t = 5$ 16 qubits $t = 15$

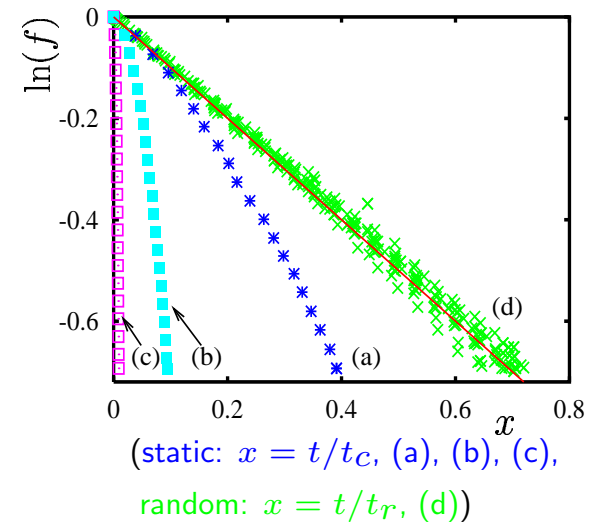


$t = 5625, \epsilon = 0$ $\epsilon = 7 \cdot 10^{-7}$
 $\hbar_{\text{eff}} = T = 2\pi/N, N = 2^{nq}$

Poincaré section ($K = kT = 1.7$)



Fidelity decay with errors



Random matrix theory for fidelity decay

Fidelity with average initial state: $f(t) = \left| \frac{1}{N} \text{tr} \left(U^{-t} \left(U e^{i\delta H_{\text{eff}}} \right)^t \right) \right|^2$

Regime $(1 - f) \ll 1$: $f(t) \approx 1 - \frac{t}{t_c} - \frac{2}{t_c} \sum_{\tau=1}^{t-1} (t - \tau) C(\tau)$

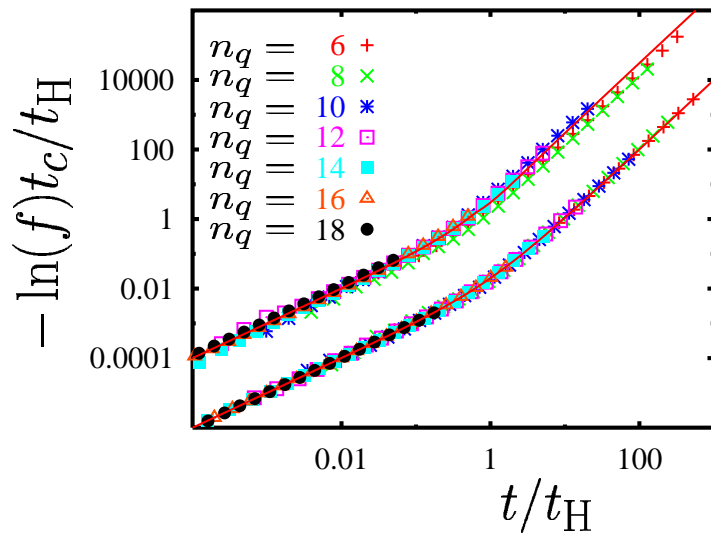
with: $\frac{1}{t_c} = \frac{1}{N} \text{tr} \left(\delta H_{\text{eff}}^2 \right)$, $C(\tau) = \frac{t_c}{N} \text{tr} \left(\underbrace{U^{-\tau} \delta H_{\text{eff}} U^{\tau}}_{\delta H_{\text{eff}}(\tau)} \delta H_{\text{eff}} \right)$

$U \in \text{COE (CUE)}$ \Rightarrow Scaling law:

$$-\langle \ln f(t) \rangle_U \approx \frac{N}{t_c} \chi \left(\frac{t}{N} \right) , \quad \chi(s) = s + \frac{2}{\beta} s^2 - 2 \int_0^s d\tilde{\tau} (s - \tilde{\tau}) b_2(\tilde{\tau}) .$$

with the “two-level form factor”: $b_2(\tilde{\tau})$.

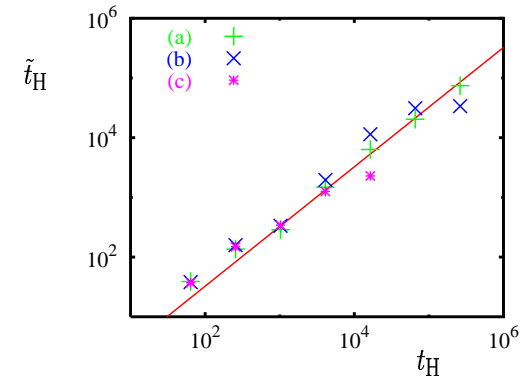
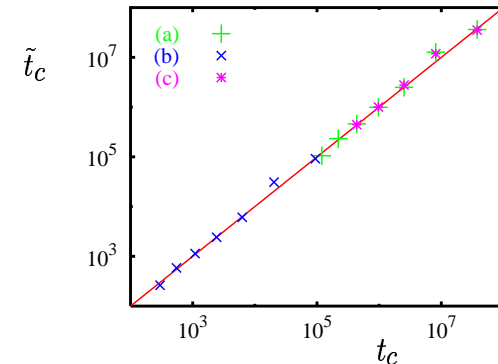
Scaling analysis for chaotic dynamics



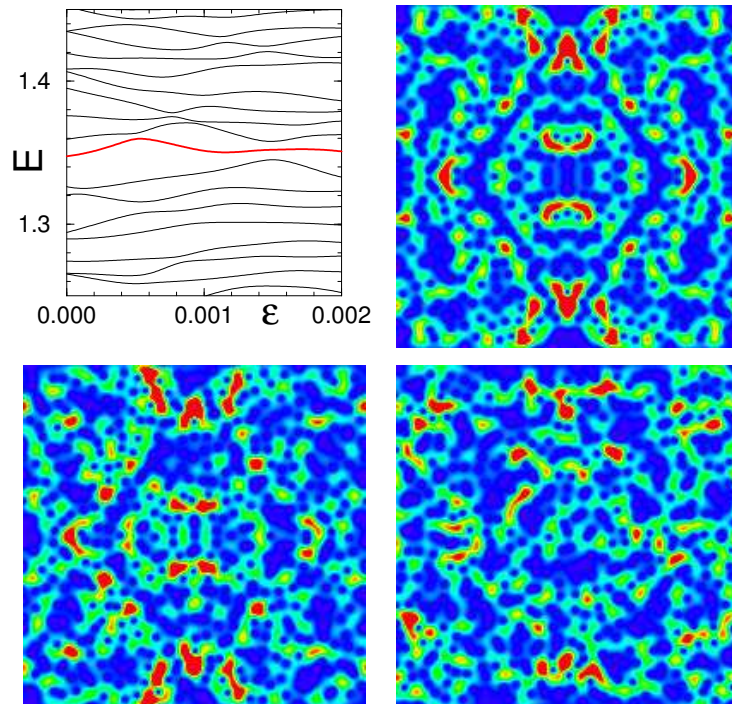
Upper curve: with theoretical values:

$$t_H = 2^{n_q} \text{ and } t_c = 1/(\varepsilon^2 n_q n_g^2)$$

Lower curve: with fit values \tilde{t}_c and \tilde{t}_H from:

$$-\ln(f(t)) = \frac{t}{\tilde{t}_c} + \frac{t^2}{\tilde{t}_c \tilde{t}_H} \quad (\tilde{t}_H \approx t_H/3)$$


Eigenstates of operating quantum computer: hypersensitivity to static imperfections



Variation of quasienergy (red curve) and corresponding eigenstate (shown by Husimi function) of unitary evolution operator of quantum sawtooth map with static imperfections strength ϵ :

$$\bar{\psi} = e^{-iT\hat{n}^2/4} e^{ik(\hat{\theta}-\pi)^2/2} e^{-iT\hat{n}^2/4} \psi = e^{-iE} \psi$$

Here $\epsilon = 0, 4 \times 10^{-4}, 10^{-3}$ (right top, left/right bottom); and $K = kT = \sqrt{2}, T = 2\pi/N, N = 2^{n_q}, J = 0, n_q = 9$. Mixing of levels takes place at critical interaction strength:

$$\epsilon_x \sim 1/\sqrt{N} \sim 2^{-n_q/2}$$

Phase diagram for the Grover algorithm with static imperfections

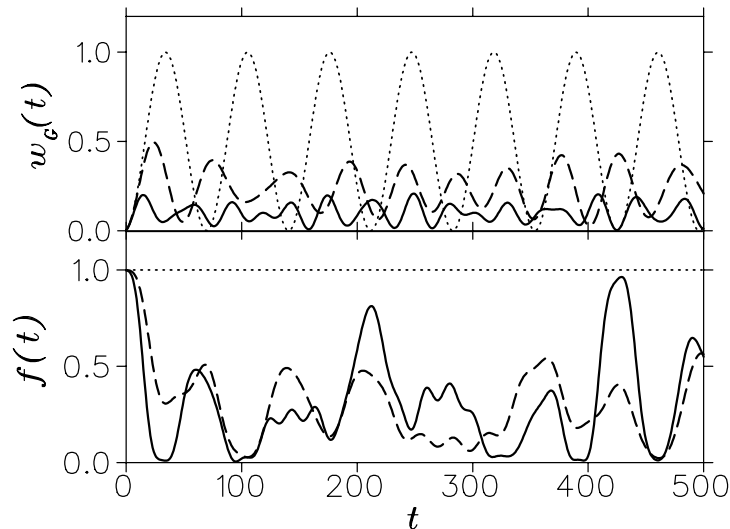
An unstructured database is presented by $N = 2^{n_q}$ states of quantum register with n_q qubits: $\{|x\rangle\}$, $x = 0, \dots, N - 1$. The searched state $|\tau\rangle$ can be identified by *oracle* function $g(x)$, defined as $g(x) = 1$ if $x = \tau$ and $g(x) = 0$ otherwise. The Grover iteration operator \hat{G} is a product of two operators: $\hat{G} = \hat{D}\hat{O}$. Here the oracle operator $\hat{O} = (-1)^{g(\hat{x})}$ is specific to the searched state $|\tau\rangle$, while the diffusion operator \hat{D} is independent of $|\tau\rangle$: $D_{ii} = -1 + \frac{2}{N}$ and $D_{ij} = \frac{2}{N}$ ($i \neq j$). For the initial state $|\psi_0\rangle = \sum_{x=0}^{N-1} |x\rangle / \sqrt{N}$, t applications of the Grover operator \hat{G} give:

$$|\psi(t)\rangle = \hat{G}^t |\psi_0\rangle = \sin((t+1)\omega_G)|\tau\rangle + \cos((t+1)\omega_G)|\eta\rangle$$

where the Grover frequency $\omega_G = 2 \arcsin(\sqrt{1/N}) \approx 2/\sqrt{N}$ and $|\eta\rangle = \sum_{x \neq \tau}^{(0 \leq x < N)} |x\rangle / \sqrt{N-1}$. Hence, the ideal algorithm gives a rotation in the 2D plane $(|\tau\rangle, |\eta\rangle)$.

The implementation of the operator D through the elementary gates requires an ancilla qubit. As a result the Hilbert space becomes a sum of two subspaces $\{|x\rangle\}$ and $\{|x + N\rangle\}$, which differ only by a value of $(n_q + 1)$ -th qubit. These subspaces are invariant with respect to operators O and D : $O = 1 - 2|\tau\rangle\langle\tau| - 2|\tau + N\rangle\langle\tau + N|$, $D = 1 - 2|\psi_0\rangle\langle\psi_0| - 2|\psi_1\rangle\langle\psi_1|$, where $|\psi_1\rangle = \sum_{x=0}^{N-1} |x + N\rangle/\sqrt{N}$ and $|\psi_{0,1}\rangle$ correspond to up/down ancilla states. Then D can be represented as $D = WRW$ (Grover (1997)), where the transformation $W = W_{n_q} \dots W_k \dots W_1$ is composed from n_q one-qubit Hadamard gates W_k , and R is the n_q -controlled phase shift defined as $R_{ij} = 0$ if $i \neq j$, $R_{00} = 1$ and $R_{ii} = -1$ if $i \neq 0$ ($i, j = 0, \dots, N - 1$). In turn, this operator can be represented as $R = W_{n_q} \sigma_{n_q-1}^x \dots \sigma_1^x \wedge_{n_q} \sigma_{n_q-1}^x \dots \sigma_1^x W_{n_q}$, where \wedge_{n_q} is generalized n_q -qubit Toffoli gate, which inverts the n_q -th qubit if the first $n_q - 1$ qubits are in the state $|1\rangle$. The construction of \wedge_{n_q} from 3-qubit Toffoli gates with the help of only one auxiliary qubit is described by A.Barenco *et al.* (1995). As a result the Grover operator G is implemented through $n_g = 12n_{tot} - 42$ elementary gates including one-qubit rotations, control-NOT and Toffoli gates. Here $n_{tot} = n_q + 1$ is the total number of qubits.

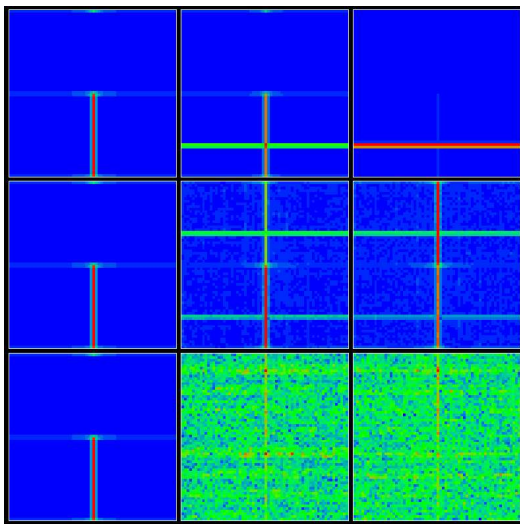
Oscillations of the Grover search probability



Probability of searched state $w_G(t)$ (top) and fidelity $f(t)$ (bottom) as a function of the iteration step t in the Grover algorithm for $n_{tot} = 12$ qubits. Dotted curves show results for the ideal algorithm ($\varepsilon = 0$), dashed and solid curves correspond to imperfection strength $\varepsilon = 4 \cdot 10^{-4}$ and 10^{-3} , respectively.

A typical example of imperfection effects on the accuracy of the Grover algorithm for a fixed disorder realization of H_S on 3×4 qubit lattice.

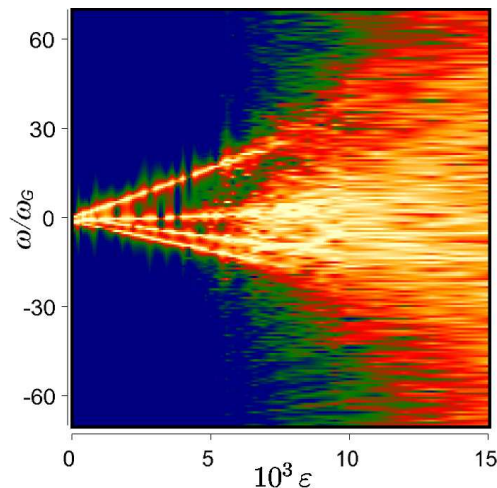
Husimi function in the Grover algorithm



Evolution of the Husimi function in the Grover algorithm at times $t = 0, 17,$ and 34 (from left to right), and for $\varepsilon = 0, 0.001,$ and 0.008 (from top to bottom). The qubit lattice and disorder realization are the same as in previous Fig. The vertical axis shows the computational basis $x = 0, \dots, 2N - 1,$ while the horizontal axis represents the conjugated momentum basis. Density is proportional to color changing from maximum (red) to zero (blue).

the probability is mainly distributed over **four states** corresponding to four straight lines in phase space: $|\tau_0\rangle = |\tau\rangle$; $|\tau_1\rangle = |\tau + N\rangle$; $|\eta_0\rangle = |\eta\rangle$; $|\eta_1\rangle = \sum_{x \neq \tau}^{(0 \leq x < N)} |x + N\rangle / \sqrt{N - 1}$

Phase diagram for spectral density

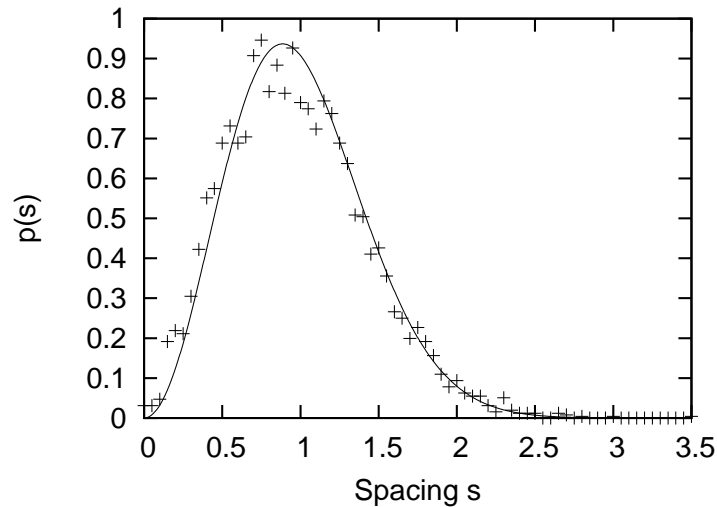


Phase diagram for the spectral density $S(\omega)$ as a function of imperfection strength ε , $n_{tot} = 12$, same disorder realization as in previous Fig. Color is proportional to density $S(\omega)$ (yellow for maximum and blue for zero).

The transition rate induced by imperfections after one Grover iteration is given by the Fermi golden rule: $\Gamma \sim \varepsilon^2 n_g^2 n_{tot}$, where n_{tot} appears due to random contribution of qubit couplings ε while n_g^2 factor takes into account coherent accumulation of perturbation on n_g gates used in one iteration. In the Grover algorithm the four states are separated from all other states by energy gap $\Delta E \sim 1$ (sign change introduced by operators O and D). Thus these four states become mixed with all others for $\varepsilon > \varepsilon_c \approx 1.7 / (n_g \sqrt{n_{tot}})$, when $\Gamma > \Delta E$.

Strong change of the period of Grover oscillations for $\varepsilon > \omega_G / (n_g \sqrt{n_q}) \propto 2^{-n_q/2}$.

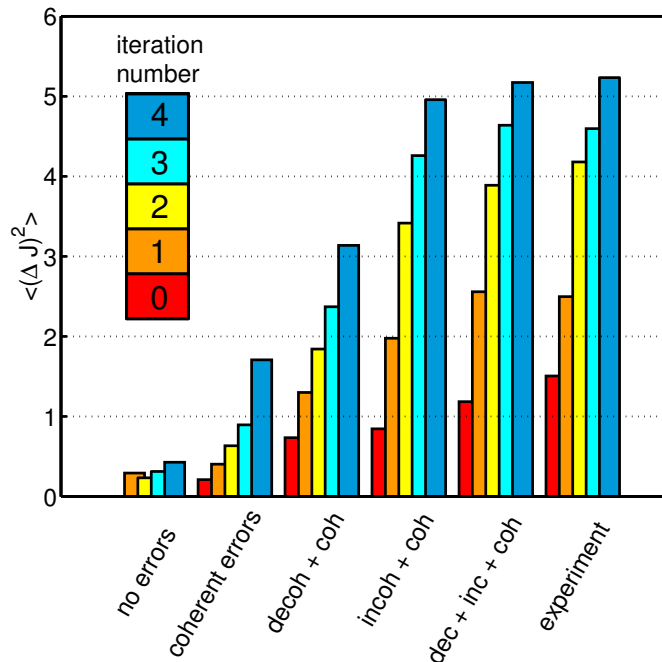
Quantum chaos in the Shor factorization algorithm



The nearest neighbor spacing distribution of eigenangles from an ensemble consisting of 5115 level spacings for the case when the first register has 10 qubits and the number to be factored is 29. The smooth curve shows the CUE distribution of random matrix theory.

- * The Shor algorithm requires exponential accuracy in spectral frequency (cf. Grover's algorithm)
- * However, in the Shor algorithm only $O(n_q^3)$ gates are used for exponentially large times
- * Similar case for the Arnold cat map (B.Georgeot, PRA **69**, 032301 (2004))
- * **Theory of imperfections effects for the Shor algorithm?**

Cory group NMR QIP Simulations of the Quantum Sawtooth Map



The second moment of the probability distribution determined from numerical simulations of the experiment including the error models discussed in the paper, compared to the ideal data and the experimental data. This plot demonstrates the relative importance of the individual noise mechanisms as they contribute to the experimentally observed delocalization process. As more errors are included in numerical simulations, the system shows stronger delocalization and more closely emulates the experimental data.

- * 3 qubit QIP based on liquid state NMR
- * Map parameters are $k = 0.27$, $K = kT = 1.5$, ($T = 5.55$),
diffusion rate $D = \pi^2 k^2 / 3 = 0.24$: regime of perturbative localization.

More about Quantum Computing

* Quantware publications and

Quantware Library of Quantum Numerical Recipes

are available at www.quantware.ups-tlse.fr

* Video Lectures on

“Quantum Information, Computation and Complexity”

at the Institut Henri Poincaré, Paris (2006):

www.lpt.irsamc.ups-tlse.fr/~dima

(click on “[video](#)” at IHP Programme QICC)